2015 American Control Conference
Palmer House Hilton
July 1-3, 2015. Chicago, IL, USA

Observability Analysis for Surface Sensor Location in Encased Battery Cells

Nassim A. Samad[1*], Jason B. Siegel[1], Anna G. Stefanopoulou[1] and Aaron Knobloch[2]

Abstract— **Compact battery pack design and cooling requirements present significant challenges for the placement of temperature sensors. Typically, temperature sensors are located near the edge of the battery, and away from the hottest regions, which leads to slower response times and increased errors in the prediction of interior cell temperature. New sensor technology allows for sensor placement between cells to improve sensor performance. With the ability to place sensors anywhere on the exterior of the cell, an observability analysis is necessary to determine the optimal locations for these sensors. The analysis is performed using a spatial discretization of a validated electrothermal model. This model describes a 5 Ah Li-ion cell harvested from a Ford C-max 2013 pack. Given that the spatial discretization of the heat partial differential equation (PDE) governing the system results in singular values that are very small (numerically zero), two methods are presented in this paper to quantify observability and address the issue of optimal sensor placement. The optimal sensor placement between cells yields a 240% improvement (for 3 sensors on the surface) and 15% improvement (for one sensor on the surface) in observability over existing sensor placement near the top edge of the cell. The pack geometry and airflow conditions impact sensor placement. It is preferable to place the sensors towards the outlet side of the airflow as opposed to the inlet side, resulting in a 13% improvement in observability.**

I. INTRODUCTION

In many engineering applications, it is important to determine the state of a system or sub-system using only partial measurements of that system. Of particular interest in hybrid electric vehicle applications is the measurement of the cell temperature in a battery pack. Monitoring temperature allows for control algorithms that can prevent excessive temperature rise and ultimately prevent thermal runways [1]. Although higher temperatures enhance the lithium transport kinetics, it is well established that excessive temperatures can also result in degradation in battery cells [2]–[4], and must be monitored.

Complex and expensive packaging and engineering schemes are required to position temperature sensors close to the regions of interest. Insertion of thermistors between battery cells is infeasable because the thickness of the sensors ($>$1mm) will cause failure or rupture of the cells due to compression on the thick sensors. However, new sensor technologies are emerging that enable the placement of temperature sensors anywhere on the cell surface at lower cost and without causing risk of battery failure. This motivates an observability analysis to determine the optimal location for a sensor on the surface of the cell. Since the core temperatures of the cell are of interest, maximizing observability, in this paper, is defined as identifying optimal sensor locations for the best estimation of the core temperatures.

Optimal sensor and actuator placement has been the focus of significant research in the controls community. The optimal locations for sensors and actuators for parabolic PDEs, which include the heat equation, have been widely investigated [5], [6]. Georges looked at the optimal sensor and actuator locations in both discrete and continuous time domains based on the observability and controllability gramians [7]. This concept of looking at observability for defining optimal sensor placements is of major importance because it allows for the best estimation of unknown system states using the sensor data. Several papers have looked at aspects of observability for PDEs [8]–[12]. Wolf et al. studied the optimal sensor placement in battery packs by performing eigen decomposition of the heat equation PDEs that govern the entire battery pack and looking at the magnitude of their corresponding eigenmodes [13]. However, little work has been done on optimal temperature sensor placements on a single battery cell.

Two methods are presented here for studying the observability and optimal temperature sensor placement on a battery cell with air flow (convection) over its surface to simulate battery pack conditions. The first is an extension to the method presented by Lim where observability is defined in terms of the projections of the eigenvectors on the observability subspace [14], while the second looks at the trace of the gramian matrix [15]. The advantage of using the first method is that it is possible to maximize observability of certain nodes of interest, such as core nodes of a battery cell. The second method looks at maximizing observability for the system as a whole and is a more traditional method of looking at observability.

II. EXPERIMENTAL CONDITIONS

A 3-cell fixture was fabricated in order to replicate a vehicle battery pack. The cells considered are prismatic hard case Lithium-Nickel-Manganese-Cobalt-Oxide (NMC) with a 5 Ah nominal capacity. Each cell has dimensions of $120mm \times 85mm \times 12.7mm$. The cells are sandwiched between two garolite end plates and bolted down to a specific preload as shown in Fig. 1. Thin film RTD (resistance temperature detector) sensors were supplied by General Electric. They are mounted between the cells for measuring spatial temperature distributions. The RTDs have a low profile,

*Corresponding author: nassimab@umich.edu
[1]Department of Mechanical Engineering, University of Michigan, 2350 Hayward Street, Ann Arbor, MI 48109-2125, USA
[2]Micro & Nano Structures Technologies, General Electric Global Research, Niskayuna, NY 12309, USA

flexible structure that allows placement between cells without obstructing airflow for cooling or possibly damaging the cells. The RTDs are fabricated on a flexible Kapton substrate and the elements are composed of Platinum (Pt) with a nominal 100 ohm resistance. The total thickness of the sensor is less than 100 microns which is 10x thinner than the current state of the art temperature sensors used on electric vehicles. The RTDs are mounted on the dimples of spacers which act as sites for holding the RTDs. The separators maintain compression whilst still allowing for airflow between the cells as shown in Fig. 1. Ambient temperature control is provided via a Cincinnati Sub-Zero ZPHS16-3.5-SCT/AC thermal chamber. Figure 1 also shows the mounting locations for the RTD sensors. There are 36 RTD sensors which span the face of the battery and are arranged in arrays of 6 temperature sensors laterally along the flow direction. A fan is used to simulate cabin air used to cool the cells. This allows the experiment to generate surface temperature profiles that are representative of those seen in the pack. When the cooling fan is off, the chamber circulates air that would result in convection over the surface of the cell with airflow velocity of $v = 0.65m/s$. A negative temperature coefficient (NTC) thermistor is mounted on top of the middle cell using the same sensor and cell location implemented in the Ford C-max 2013 pack. This allows for comparing observability of the current sensor to the placement of the RTD sensors over the surface.

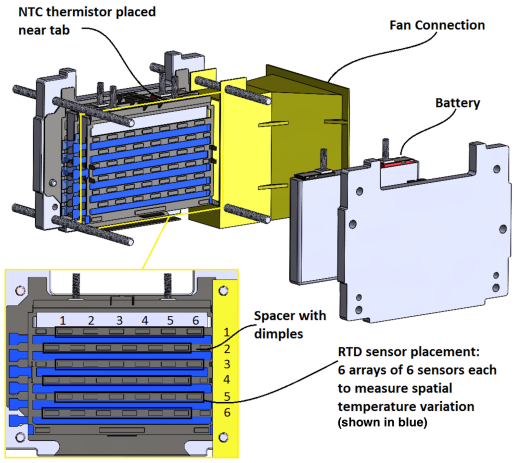

Fig. 1. Exploded view of the fixture showing locations of temperature sensors on the surface of the battery

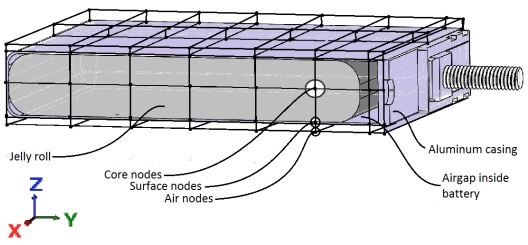

Fig. 2. Schematic of the 5 layered n× m mesh used for the thermal model

III. SENSOR PLACEMENT MODEL

A. Thermo-electric model

A thermo-electric model, as presented in [16], is being considered here. The model consists of a 3-D thermal network coupled to a distributed equivalent circuit model as shown in Fig. 2. The core nodes in Fig. 2 represent the lumped properties of the jelly roll, while the surface nodes represent the aluminum casing of the cell with thickness $0.6mm$. The cell also has air gaps between the jelly roll and the casing which are modeled using the air thermal properties. Since air is flowing over the surface of the cell, the air nodes on top of the surface of the cell have to be also modeled. The overall heat transfer equation applies to each node in the cell:

$$\rho c V \frac{dT}{dt} = \dot{Q}_{gen} + \dot{Q}_{in} - \dot{Q}_{out}. \tag{1}$$

where ρ is the density of the node volume, c is the specific heat capacity, and V the volume of that node. $\dot{Q}_{gen}$ is the heat generation, and $\dot{Q}_{in} - \dot{Q}_{out}$ is the net heat transfer into the node volume. The heat generation is defined as:

$$\dot{Q}_{gen} = \begin{cases} I^2 R_s + \frac{V_1^2}{R_1} + \frac{V_2^2}{R_2} + IT\frac{dU}{dT} & \textit{jelly roll node.} \\ 0. & \textit{other nodes} \end{cases} \tag{2}$$

Note that for an interior node, the first 3 terms of the heat generation equation represent ohmic heat losses, while the last term represents the entropic heat generation. The entropic heat generation $\frac{dU}{dT}$ is constant as a function of temperature but varies with state of charge (SOC). Since the analysis is done around a nominal SOC, $\frac{dU}{dT}$ is assumed to be constant. The net heat transfer for an interior node (with temperature T_i) is:

$$\begin{aligned}(\dot{Q}_{in} - \dot{Q}_{out})_{core} = &\sum \frac{K_{xy} A_{xy}}{L_{xy}} (T_{xy,i} - T_i) \\ &+ \sum \frac{K_z A_z}{L_z} (T_{z,i} - T_i).\end{aligned} \tag{3}$$

The net heat transfer for all surface nodes is:

$$\begin{aligned}(\dot{Q}_{in} - \dot{Q}_{out})_{surf} = &\sum \frac{K_{xy} A_{xy}}{L_{xy}} (T_{xy,i} - T_i) \\ &+ \sum \frac{K_z A_z}{L_z} (T_{z,i} - T_i) \\ &+ h_{surf} A_{surf} (T_{air,i} - T_i).\end{aligned} \tag{4}$$

Finally the net heat transfer for the airflow nodes is defined as:

$$\begin{aligned}(\dot{Q}_{in} - \dot{Q}_{out})_{air} = &\, h_{surf} A_{surf} (T_{surf,i} - T_i) \\ &+ (\rho c)_{air} A_{gap} v (T_{air,in} - T_{air,out}).\end{aligned} \tag{5}$$

where K is the thermal conductivity and h is the heat transfer coefficient. A and L are the corresponding areas and lengths between neighboring volumes. $T_{xy,i}$ and $T_{z,i}$ are the temperatures of the surrounding nodes in the $xy-plane$ and $z-direction$ consecutively, and v is the velocity of air.

The thermal properties used in equations 1 through 5 are summarized in Table I.

TABLE I

IDENTIFIED THERMAL PARAMETERS

Parameter	Jelly roll	Aluminum casing	Air gaps
$K_{xy}[\,W/m^2K]$	22	237	0.024
$K_z[\,W/m^2K]$	1.7	237	0.024
$h_{surf}[\,W/mK]$	—	45	—
$h_{edge}[\,W/mK]$	—	18	—
$(\rho c)[\,J/m^3K]$	2.75e6	2.42e6	1200

B. State-Space Representation

The model presented in section III-A is nonlinear. The nonlinearity is present in the form of temperature dependent resistances (R_s, R_1 and R_2), and entropic heat generation $IT\frac{dU}{dT}$. For any given profile or excitation input, the steady state value is found using the non-linear model, and linearization is done around that steady state value for both the temperature dependent resistances (R_s, R_1 and R_2), and the entropic heat generation $IT\frac{dU}{dT}$, where for the resistance:

$$R(T) = R(T_{eq}) + \left.\frac{\partial R}{\partial T}\right|_{T_{eq}} (T - T_{eq}). \tag{6}$$

and for the entropic heat generation $f(I^2, T) = IT\frac{dU}{dT}$:

$$f(I^2,T) = f(I^2_{eq}, T_{eq}) + \frac{\partial f}{\partial I^2}(I^2 - I^2_{eq}) + \frac{\partial f}{\partial T}(T - T_{eq}). \tag{7}$$

where $\frac{\partial f}{\partial I^2}$ is calculated as:

$$\frac{\partial f}{\partial I^2} = \frac{1}{2I_{eq}}(T_{eq}\frac{dU}{dT}). \tag{8}$$

Note that linearization is done with respect to I^2 and T since I^2 is an input to the system, and T is a state variable. Accordingly, the system can thus be written in state space representation as:

$$\begin{aligned} \dot{\mathbf{T}} &= A\mathbf{T} + B\mathbf{u}. \\ \mathbf{y} &= C\mathbf{T}. \end{aligned} \tag{9}$$

Where $\mathbf{T} = [T_1, T_2, ..., T_n]^T$ is the matrix of state variables of temperatures at each node and $\mathbf{u} = [I^2, T_{amb}]^T$ is the input to the system. A and B are the system matrices that correspond to linearizing equations 1 through 8, and C is a matrix defining the locations of sensors on the system, and thus the observable output $\mathbf{y}$, where:

$$C = \begin{bmatrix} 0 & 1 & ... & 0 \end{bmatrix}. \tag{10}$$

indicates that, for example, only one sensor at node 2 is placed.

C. Sensor placement and observability

Several methods have been proposed for studying the observability of ODEs and addressing the issue of optimal sensor placement. The most common metric is the condition number or minimum singular values of the observability gramian matrix W^o. However, for studying the observability of the heat equation, it has been shown that increasing the number of modes of a system will rapidly decrease the value of the smallest eigenvalue, σ^N_{min}, of the observability gramian matrix implying weak observability [17]. After N=8 modes, the smallest eigenvalue, σ^N_{min}, is almost zero. For heat transfer problems, one would be interested in looking at the observability of certain modes or eigenvalues instead of all the eigenvalues of the system. Hence, a different approach for looking at observability has to be established.

Two methods for quantifying sensor placement are analyzed and compared. The first method is based on analyzing the trace of the observability gramian matrix similar to the work done by Fang et al. [15]. This method leverages the fact that a larger trace of the observability gramian matrix W^o tends to result in a higher rank for the matrix [18]. The other method is based upon the work by Lim [14], where optimal sensor placement is found using the orthogonal projections of the eigenmodes onto the observable subspace. This method is expanded upon by studying the projections of certain eigenmodes that are of interest to the application. Thus maximizing the observability of certain nodes instead of the system as a whole.

1) Trace analysis: For the system defined in Section III-B, and for a chosen sensor location as defined by matrix C_i, the observability gramian matrix W^o_i is defined as:

$$W^o_i = \int_0^\infty e^{A^T\tau} C_i^T C_i e^{A\tau} d\tau. \tag{11}$$

The trace of the matrix W^o_i is defined as:

$$tr(W^o_i) = \sum_{j=1}^{n} \lambda_{ij}(W^o_i). \tag{12}$$

where $\lambda_{ij}(W^o_i)$ are the eigenvalues of W^o_i, with corresponding eigenvectors $\phi_{ij}(W^o_i)$.

2) Eigenmode projections: The method presented expands upon Lim [14] to achieve maximum observability for certain critical nodes of interest. Given the system presented in Section III-B, a given matrix C_i for the locations of sensors and the resulting observability gramian matrix W^o_i presented in section III-C.1, one can decompose W^o_i into its eigen decomposition, which would be written as:

$$W^o_i = [U_i \quad U_i^\perp] \begin{bmatrix} \sum_i^o & \\ & 0 \end{bmatrix} \begin{bmatrix} U_i^T \\ U_i^{\perp T} \end{bmatrix}. \tag{13}$$

where U_i is a matrix with column vectors that form an orthogonal basis for matrix W^0_i, and $\sum_i^o = diag(\lambda_{i,1}, \lambda_{i,2}, ..., \lambda_{i,q})$ is a diagonal matrix of the eigenvalues of W^o_i (where $\lambda_{i,1} \geq \lambda_{i,2} \geq ... \geq \lambda_{i,q}$), and q is the rank of the gramian matrix W^o_i or the dimension of matrix U_i (the threshold for defining the rank is set by default at 9.2×10^{-13} using MATLAB). As outlined in [14], the projection of the eigenvectors, ϕ_{ij}, corresponding to eigenvalues λ_{ij} onto the subspace U_i is:

$$\phi^{proj}_{ij} = U_i(U_i^T U_i)^{-1} U_i^T \phi_{ij}. \tag{14}$$

A scalar, α_{ij}, is defined to reflect the relative significance of the corresponding eigenvector ϕ_{ij}, where:

$$\alpha_{ij} = \phi^{proj^T}_{ij} W^o_i \phi^{proj}_{ij}. \tag{15}$$

Equation 15 implies that α_{ij} takes a larger value when the projected eigenvector, ϕ_{ij}^{proj}, is in the direction of maximum observability. However, since the nodes corresponding to the jelly roll inside the cell are of interest, and observing those nodes is critical, the method presented in [14] is expanded to look at the observability of those critical nodes by analyzing the contribution of the corresponding eigenmodes of those nodes. This expansion of Lim's method is shown in the eigenvalue plot of system matrix A in Fig. 3. The plot in Fig. 3 corresponds to the eigenvalues when only chamber fan is turned on to maintain ambient temperature (resulting in a flow rate of $v = 0.65m/s$ over the surface of the cell). This analysis however could be performed for different ambient and flow conditions.

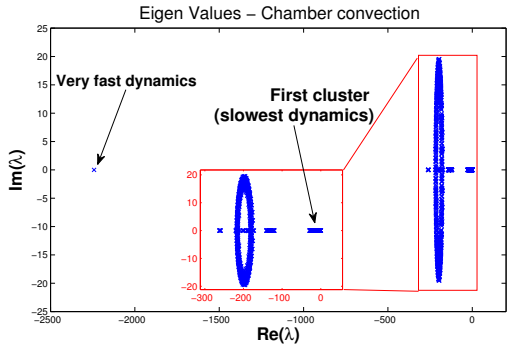

Fig. 3. Eigenvalue plot of system matrix A

Since each eigenvector corresponding to each eigenvalue in the system represents the contribution of the different states to that eigenvalue, a criteria is established to identify the states that contribute most to the eigenvalues of interest. It is also required that at least the states corresponding or contributing to the slowest dynamics in the system are observed. A procedure for doing such an analysis is outlined below:

Step 1: Choose eigenvalues of interest

1) Perform eigen decomposition on system matrix A.
2) For any given eigenvalue, quantify the contribution (β_{ij}^k) of each state to that specific eigenvalue according to:

$$\beta_{ij}^k(\%) = \frac{\left|\phi_{ij}(k)\right|}{\sum_{k=1}^{n_s}\left|\phi_{ij}(k)\right|} \times 100. \qquad (16)$$

Equation 16 above implies that for a given sensor placement represented by matrix C_i, and for a given eigenvalue λ_{ij} with corresponding eigenvector ϕ_{ij}, β_{ij}^k (for k= 1 , ... , n_s = number of states) will represent the contribution of state k to eigenvalue λ_{ij}.
3) Choose the eigenvalues for which the states of interest (such as the core nodes) have the highest mean β_{ij}^k. The eigenvectors, ϕ_{ij}, corresponding to those eigenvalues, λ_{ij}, will be projected onto subspace U_i for observability analysis. This tailors the solution towards maximizing the observability of those states instead of the system as a whole.

Step 2: Perform observability

1) Find parameter α_{ij} for each eigenvector of the eigenvalues chosen in *Step 1* above using Eq. 15.
2) Define a final metric, γ_{ij}, for quantifying the degree of observability of the chosen eigenmodes using a given sensor placement represented by matrix C_i, using the $\mathcal{L}_2$ norm of α_{ij}:

$$\gamma_i = \left\|\alpha_{ij}\right\|. \qquad (17)$$

where j = 1, 2, ..., n_e sweeps the number of eigenvalues of interest, and i = 1, 2, ..., n_c sweeps the number of possible sensor placements.

IV. RESULTS

In this section, the results of the trace and eigenmode projection methods are summarized for a given flow rate condition over the surface of the cell (chamber fan convection only). For easier analysis of sensor placement, 23 ×18 nodes were chosen such that they coincide with sensor locations (or dimple locations) as shown in Fig. 4. In total, there are 23×18×5 = 2070 nodes. Figure 4 shows that there are 36 possible sensor locations on the surface of the battery.

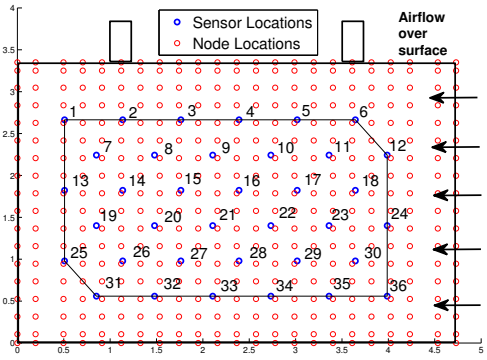

Fig. 4. Locations of sensors and nodes on the surface of the battery

Analysis is divided into two parts: one sensor analysis, and a strip of 3 sensor analysis. The first analysis highlights the advantage of using sensors placed on the surface as opposed to a thermistor placed closer to the tab (like the Ford C-max placement). The second analysis identifies an optimal location for placing a strip of 3 sensors. However, for the eigenmode projections method, certain eigenvalues of interest have to be chosen first. As shown in Fig. 3, a threshold or cutoff is set to chose the eigenvalues with slow dynamics and those for which the jelly roll states contribute the most. A plot of parameter β_{ij}^k as a function of the first x number of eiegnvalues is shown in Fig. 5. The plot shows that choosing the first 303 slowest eigenvalues and their corresponding eigenmodes captures the slowest dynamics of the battery and constitutes the highest contribution from the jelly roll states. Accordingly, only the first 303 slowest eigenvalues are chosen for the eigenmode projections method that is summarized in sections IV-A and IV-B.

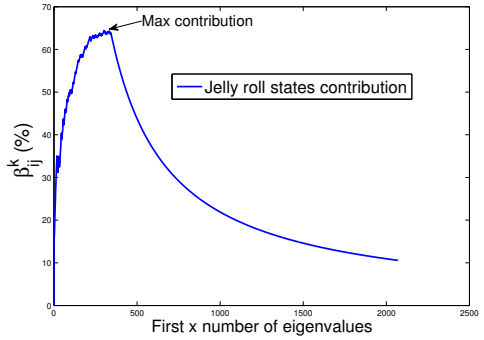

Fig. 5. Jelly roll states contribution to first x slowest eigenvalues

A. One sensor analysis

Figure 6 shows the trace and γ values for a sensor permuted across all dimple locations (36 dimple locations). This shows that the trace and eigenmode projections method exhibit the same trends but differ slightly in the location of best observability. This could be due to the fact that the trace takes into account all the eigenvalues of the system, while the eigenmode projection method only takes into account some eigenvalues of interest. Moreover, comparing the best location of one sensor on the surface to a conventional sensor placed near the tabs shows that observability is higher for a sensor on the surface than it is for one near the tabs as shown in Table II.

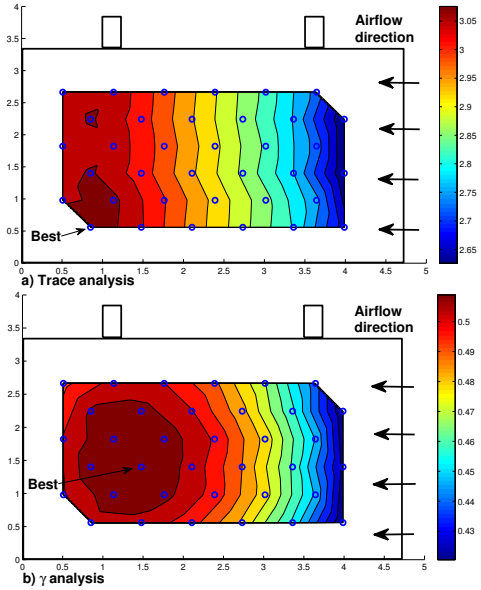

Fig. 6. Trace and γ based on a single sensor approach

TABLE II

ONE SENSOR SUMMARY

Method	Surface	Near tab	%Improvement
Trace	3.109	2.685	15.79
Eigenmode projection	0.515	0.436	18.12

B. Three sensor analysis

Sensors provided by GE are inline on a Kapton strip such that they span dimples in the same row. Given this constraint, the results of the three sensor permutation is summarized in Fig. 7. Similar to to the results from section IV-A, it can be seen that the best locations for sensors using the trace and eigenmode projection methods are closer to the airflow outlet side, with the worst positions towards the airflow inlet side. Moreover, Table III shows the percent improvement in observability if 3 sensors are used on the surface as compared to a traditional sensor placed near the tabs. There is a huge improvement for using 3 sensor on the surface instead of 1 sensor near the tabs (240% improvement). Up to 13% improvement could be achieved when placing sensors closer to the outlet as opposed to the inlet side of the airflow. This is also true for the one sensor analysis where the best locations are at positions 31 (using trace analysis in Fig. 6a) and 20 (using eigenmode projection method in Fig. 6b). This is an obvious observability result since the highest observability measures collocate with the highest measured surface temperatures as shown in Fig. 8.

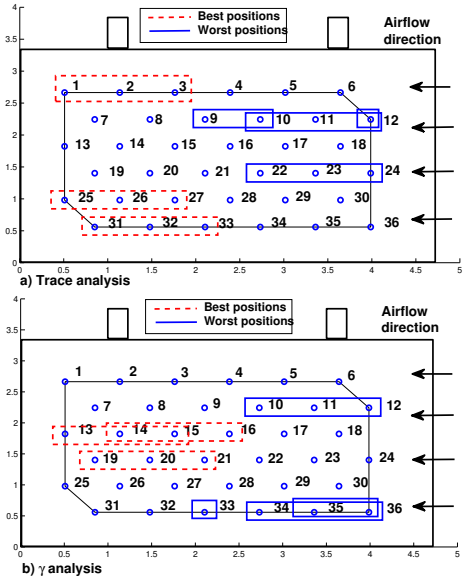

Fig. 7. Best and worst positions for three sensors using trace and γ analysis

TABLE III

THREE SENSOR SUMMARY

Method	γ (surface)	γ (near tab)	%Improvement
Trace	9.168	2.685	241
Eigenmode projection	1.535	0.436	252

V. CONCLUSIONS

Two methods for looking at the observability of a thermal model for a battery cell using novel thin RTD temperature sensors have been analyzed. Results show that sensors placed

over the surface of the battery provide better observability as compared to a conventional sensor placed on top of the battery (near the tabs in the Ford C-max 2013 pack). The analysis is done by looking at the trace of the observability gramian matrix and at the projection of the eigenmodes of the system matrix onto the observability subspace. A 15.79/18.12% improvement (trace method / eigenmode projection method) could be achieved if one sensor is placed at the optimal location on the surface of the battery as compared to a sensor placed on top of the battery. 241/252% improvement (trace method / eigenmode projection method) improvement could be achieved if 3 sensors are used. Results also indicate that better observability could be achieved if the sensors are placed closer to the outlet side of the airflow as opposed to the inlet side. Although the results from both methods are not entirely the same, the overall trend from both methods indicates that placing the sensors at the hot spot location results in best observability. For the experimental conditions presented above, the eigenmode projection method provides a better match. However, further experiments are required to verify the adequacy of both methods.

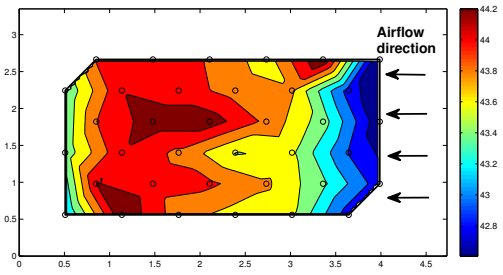

Fig. 8. Experimental surface temperature profiles for a 50A charge sustaining pulsing experiment

ACKNOWLEDGMENT

The information, data, or work presented herein was funded in part by the Advanced Research Projects Agency-Energy (ARPA-E), U.S. Department of Energy, under Award Number DE-AR0000269[1]. The authors would like to acknowledge the contribution of Jason Karp and Christopher Kapusta from GE Global Research and the GE Global Research cleanroom staff, Brian Engle and David Villella from Amphenol Advanced Sensors for providing the RTD sensors and for their continuous feedback and support, and Dyche Anderson from Ford Motor Company.

[1]Disclaimer: The information, data, or work presented herein was funded in part by an agency of the United States Government. Neither the United States Government nor any agency thereof, nor any of their employees, makes any warranty, express or implied, or assumes any legal liability or responsibility for the accuracy, completeness, or usefulness of any information, apparatus, product, or process disclosed, or represents that its use would not infringe privately owned rights. Reference herein to any specific commercial product, process, or service by trade name, trademark, manufacturer, or otherwise does not necessarily constitute or imply its endorsement, recommendation, or favoring by the United States Government or any agency thereof. The views and opinions of authors expressed herein do not necessarily state or reflect those of the United States Government or any agency thereof.

REFERENCES

[1] B. K. Mandal, A. K. Padhi, Z. Shi, S. Chakraborty, and R. Filler, "Thermal runaway inhibitors for lithium battery electrolytes," *Journal of Power Sources*, vol. 161, no. 2, pp. 1341 – 1345, 2006.

[2] P. Ramadass, B. Haran, R. White, and B. N. Popov, "Capacity fade of sony 18650 cells cycled at elevated temperatures: Part i. cycling performance," *Journal of Power Sources*, vol. 112, no. 2, pp. 606 – 613, 2002.

[3] R. Wright, J. Christophersen, C. Motloch, J. Belt, C. Ho, V. Battaglia, J. Barnes, T. Duong, and R. Sutula, "Power fade and capacity fade resulting from cycle-life testing of advanced technology development program lithium-ion batteries," *Journal of Power Sources*, vol. 119121, no. 0, pp. 865 – 869, 2003.

[4] J. Shim, R. Kostecki, T. Richardson, X. Song, and K. Striebel, "Electrochemical analysis for cycle performance and capacity fading of a lithium-ion battery cycled at elevated temperature," *Journal of Power Sources*, vol. 112, no. 1, pp. 222 – 230, 2002.

[5] A. Armaou and M. A. Demetriou, "Optimal actuator/sensor placement for linear parabolic {PDEs} using spatial norm," *Chemical Engineering Science*, vol. 61, no. 22, pp. 7351 – 7367, 2006.

[6] M. Demetriou, "Numerical investigation on optimal actuator/sensor location of parabolic pdes," in *American Control Conference, 1999. Proceedings of the 1999*, vol. 3, 1999, pp. 1722–1726 vol.3.

[7] D. Georges, "The use of observability and controllability gramians or functions for optimal sensor and actuator location in finite-dimensional systems," in *Decision and Control, 1995., Proceedings of the 34th IEEE Conference on*, vol. 4, Dec 1995, pp. 3319–3324 vol.4.

[8] T. Duyckaerts, X. Zhang, and E. Zuazua, "On the optimality of the observability inequalities for parabolic and hyperbolic systems with potentials," *Annales de l'Institut Henri Poincare (C) Non Linear Analysis*, vol. 25, no. 1, pp. 1 – 41, 2008.

[9] S. Cohn and D. Dee, "Observability of discretized partial differential equations," *SIAM Journal on Numerical Analysis*, vol. 25, no. 3, pp. 586–617, 1988.

[10] J. Ng, S. Dubljevic, and I. Aksikas, "Aspects of controllability and observability for time-varying pde systems," in *American Control Conference (ACC), 2012*, June 2012, pp. 2220–2225.

[11] Y. Sakawa, "Observability and related problems for partial differential equations of parabolic type," *SIAM Journal on Control*, vol. 13, no. 1, pp. 14–27, 1975.

[12] D. Halim and S. R. Moheimani, "An optimization approach to optimal placement of collocated piezoelectric actuators and sensors on a thin plate," *Mechatronics*, vol. 13, no. 1, pp. 27 – 47, 2003.

[13] P. Wolf, S. Moura, and M. Krstic, "On optimizing sensor placement for spatio-temporal temperature estimation in large battery packs." in *CDC*, 2012, pp. 973–978.

[14] K. B. Lim, "Method for optimal actuator and sensor placement for large flexible structures," *Journal of Guidance, Control, and Dynamics*, vol. 15, no. 1, pp. 49–57, Jan. 1992.

[15] H. Fang, R. Sharma, and R. Patil, "Optimal sensor and actuator deployment for hvac control system design," in *American Control Conference (ACC), 2014*, June 2014, pp. 2240–2246.

[16] N. A. Samad, J. B. Siegel, and A. G. Stefanopoulou, "Parameterization and validation of a distributed coupled electro-thermal model for prismatic cells," in *DSCC(2014)*.

[17] W. Kang, L. Xu, and F. X. Giraldo, "Partial Observability and its Consistency for PDEs," *ArXiv e-prints*, Dec. 2014.

[18] M. Fazel, H. Hindi, and S. Boyd, "Rank minimization and applications in system theory," in *American Control Conference, 2004. Proceedings of the 2004*, vol. 4, June 2004, pp. 3273–3278 vol.4.